Journal of Atomic and Molecular Sciences

ISSN 2075-1303

Global Science Press

Theoretical insights into the excited state hydrogen bond and ESIPT reaction for 2-amino-3-(2'-benzoxazolyl)quinoline and 2-amino-3-(2'-benzothiazolyl)-quinoline

Received Apr.25, 2018,
Accepted Aug. 13, 2018,

DOI: 10.4208/jams.042518.081318a

http://www.global-sci.org/jams/

Qiaoli Zhang[1], Guang Yang[2], Xiaoyan Song[1], Jinfeng Zhao[3],*, Dapeng Yang[1,3,]*

Abstract. Two N-H type excited state intramolecular proton transfer (ESIPT) systems (i.e., 2-amino-3-(2'-benzoxazolyl)quinoline (ABO) and 2-amino-3-(2'-benzothiazolyl)-quinoline (ABT)) have been investigated. Adopting DFT and TDDFT methods coupling with B3LYP functional and TZVP basis set, our simulations about ABO and ABT molecules have successfully reappeared experimental results, based on which the rationality of our calculations is confirmed. Using Atoms in Molecules (AIM) analytical method, we firstly explore the interactions about chemical bond and verify the formation of hydrogen bond N-H•••N for ABO and ABT in the S_0 state. Investigating the primary geometrical parameters involved in N-H•••N, we find it should be strengthened in the S_1 state. Upon photoexcitation, charge transfer phenomenon is found via frontier molecular orbitals (MOs), and charge redistribution provides the tendency of ESIPT reaction for ABO and ABT. According to our constructed potential energy curves of both S_0 and S_1 states for ABO and ABT using two kinds of methods (i.e., the elongation of N-H single bond and the weakening of H•••N hydrogen bond), we clarify the ESIPT mechanisms and explain the recovery of four-level reaction cycle. Our searching transition state (TS) structures and simulated intrinsic reaction coordinate (IRC) path further confirm the ESIPT reaction.

Keywords: Weak Interaction; Hydrogen Bond; ESIPT; Charge Redistribution.

1. Introduction

It is well known that hydrogen bond should be one of the most primary weak interactions in natural world, which makes our life-cycle to be sustained in the world [1-3]. Hydrogen bonds play significant roles in stabilization of the secondary structures of biomolecules such as proteins, DNA, RNA, and so on. Generally speaking, a double effect can be found in biological systems. On one hand, in the form of strong directional interaction, it can result in the stable supramolecular architectures that are inevitable for the construction of elementary building blocks of our life. One the other hand, it can serve as an active site for the occurrence of a vista of interactions. Thus the investigations about hydrogen bonding interactions would be vital to delve into the critical evaluation of many phenomenon occurring in crystal, in solvent phase, and in living organisms [4-6]. As a fundamental class of photochemistry, proton transfer (PT) is ubiquitous as an elementary reaction throughout nature [7], which occurs along with a pre-existing intra- or inter- molecular hydrogen bond wire. Generally, the photo-induced solvent-solute PT processes could be considered to become a series of fundamental steps, as described by Eigen-Weller mechanism, i.e., the electronic redistribution, ion-pair formation, hydrogen bonding rearrangement processes [8, 9]. Recently, with the perpetual development of experimental techniques and measure, more and more attention has turned to the excited state dynamical behaviors. By the light of nature, excited state intra- or inter- molecular proton transfer (ESIPT) reactions have attracted much attention [10-19].

To the best of knowledge, the ESIPT represents a complicated photo-tautomerization process and usually involves the transfer of a hydroxyl/imino proton from the pre-existing hydrogen bond wire to the oxygen or nitrogen acceptor in the excited state, which can lead to a new isomer dubbed as the proton-transfer tautomer or the photo-tautomer [20-25]. Basically, upon the photo-excitation process, the normal stable ground-state structure (enol) could be excited to the excited state. After the thermal relaxation, the most stable form (enol*) in the S_1 state should be formed with

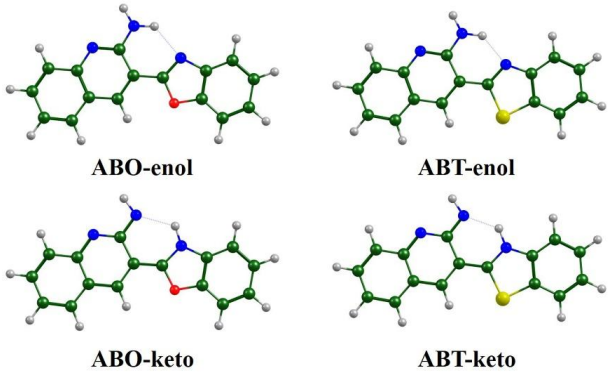

Figure 1: View of the geometrical structures of ABO-enol, ABO-keto, ABT-enol and ABT-keto. Herein, Green: C atoms; Gray: H atoms; Blue: N atoms; Red; O atoms; Greenyellow: S atoms.

[1.] *School of Mathematics and Statics, North China University of Water Resources and Electric Power, Zhengzhou 450046, China*
[2.] *Basic Teaching Department, Jiaozuo University, Jiaozuo 454000, China*
[3.] *State Key Laboratory of Molecular Reaction Dynamics, Theoretical and Computational Chemistry, Dalian Institute of Chemical Physics, Chinese Academy of Sciences, Dalian 116023, China*
Corresponding authors: Email: dpyang_ncwu@163.com;
Email: jfzhao1990112@163.com.

the normal fluorescence. In the process of the ESIPT reaction, enol* can convert into the excited photo-tautomer (keto*). And the keto* structure can be recognized by emission spectrum in experiment due to the longer wavelength fluorescence (the Stokes shift can be as large as 8000 ~ 12000 cm^{-1}) [26-30]. Due to the drastic structural alternations, the photo-tautomers keto* owns different photochemical and photophysical properties from that of the initial enol* species. Just due to the novel characteristics of keto* structure, great versatilities could be offered in varieties of applications, such as lasing materials, fluorescent sensors, photostabilizers, solid state emitters, and so on [31-38].

In fact, in the field of ESIPT reactions, most of them refer to the O-H type hydrogen bond. And the investigations indicate that only a few reports have reported the amino-type ESIPT using amine as the proton donors [39-45]. Generally, the amino proton owns much weaker acidity than the hydroxyl proton in the S_0 state [46]. And a similar acidity tendency is expected in the excited states; therefore, the ESIPT rarely occurs in the N-H hydrogen bonding systems unless the acidity of N-H can be enhanced via suitable chemical modifications. Particularly, Chou and coworkers have detailed investigated this aspect in recent years [47-49]. Based on different electron-withdrawing and electron-donor groups, the ESIPT process along with N-H hydrogen bonding wires might be harnessed. Khimich et al. designed and explored the absorption and emission spectra as well as the relative fluorescence quantum yields about two systems (i.e., 2-amino-3-(2′-benzoxazolyl)quinoline (ABO) and 2-amino-3-(2′-benzothiazolyl)-quinoline (ABT)) experimentally [50]. The N-H type ESIPT reactions might exist in ABO and ABT system. And recently, Khimich et al. further investigated the steady-state spectra of ABO and ABT structures under different temperatures and confirmed the different photochemical properties bringing from temperatures [51, 52], while the detailed ESIPT mechanism for both ABT and ABO is absent. To the best of our knowledge, the experimental spectroscopic techniques could just provide the one-sided information about excited state behaviors such as the photophysical and photochemical properties. Further, as a kind of N-H type ESIPT systems, the excited state processes of ABO and ABT might be modified via chemical positions, which may facilitate other applications in future. Thus, as the fundamental aspect, the specific ESIPT mechanism and process for ABO and ABT structure should be principle.

To explore and clarify the explicit excited state dynamical behaviors for both ABO and ABT system, in this present work, a detailed quantum chemical computational calculations have been performed. Adopting density functional theory (DFT) and time-dependent density functional theory (TDDFT) methods, we mainly focus on the fundamental aspects concerning the different electronic states and relative structures involved in the ESIPT reactions. And the remainder of this paper can be organized such that the next section describes the theoretical details. Section 3 presents the discussions and results about ABO and ABT systems including the geometrical analyses, electronic spectra, the charge distributions and potential energy curves. And lastly, a final section provides a summary and conclusion of this present work.

2. Computational Methods

All the calculations have been carried out using DFT and TDDFT methods with the Becke's three-parameter hybrid exchange function with the Lee-Yang-Parr gradient-corrected correlation functional (B3LYP) [53-55] as implemented in the Gaussian 09 program [56]. And after testing basis sets, the triple-ζ valence quality with one set of polarization function (TZVP) has been

Table 1. The calculated bond lengths (Å) and angles (º) involved in intramolecular hydrogen bond N-H•••N for ABO-enol, ABO-keto, ABT-enol and ABT-keto forms in S_0 and S_1 states based on the DFT//TDDFT B3LYP/TZVP theoretical level.

	ABO-enol		ABO-keto		ABT-enol		ABT-keto	
	S_0	S_1	S_0	S_1	S_0	S_1	S_0	S_1
N-H	1.010	1.025	1.010	2.009	1.011	1.028	1.011	1.880
H···N	2.015	1.918	2.015	1.021	1.971	1.861	1.971	1.030
δ(N-H···N)	130.9	134.5	130.9	122.8	131.0	135.6	131.0	130.4

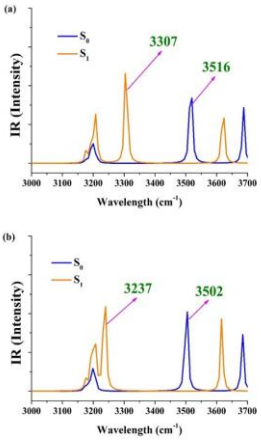

Figure 2: The calculated IR spectra of N-H vibrational mode for ABO-enol (a) and ABT-enol (b) systems in both S_0 and S_1 states under the DFT//TDDFT/B3LYP/TZVP theoretical level.

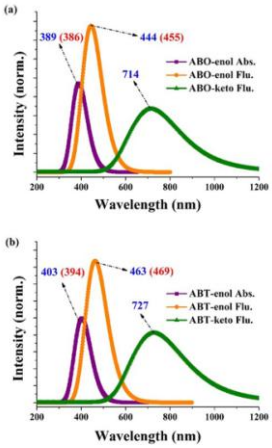

Figure 3: Our calculated absorption and emission spectra of ABO and ABT systems based on the TDDFT/B3LYP/TZVP theoretical level. Herein, the blue values indicate our theoretical results and the red values in brackets stand for the experimental results

selected [57]. The optimizations of ground-state structures are performed using DFT method, and the calculations about excited state are based on TDDFT method. No constrain of bond lengths, bond angles or dihedral angles have been adopted in this present work expect for additional remarks. And the infrared vibrational frequencies have been also analyzed to confirm that all the structures correspond to the local minima on S_0 and S_1 state potential energy surfaces. The harmonic vibrational frequencies with normal mode force constants, anharmonic vibrational frequencies with normal mode force constants, dipole moments, and dipole moment first derivatives have been calculated for all the optimized structures. And solution phase (ethanol) calculations have been also carried out using the polarizable continuum model according to the integral equation formalism (IEFPCM) with atomic radii cavity definitions according to the universal force field model as implemented in Gaussian 09 [58-60]. The results from solution phase calculations have been obtained from complexes that are geometry optimized in the PCM reaction field. PCM models mitigate the computational burden of explicitly modeling solvent molecules and the specific interactions with the solute. And the solvent can be treated as a constant dielectric reaction field where the charge density of the solute is projected onto a grid on the surface of a solvent cavity and polarized depend on the value of the solvent dielectric. The calculations about the vertical excitation energies have been carried out from the optimized structures of the S_0 state. And six low-lying absorbing transitions have been predicted in this work. All of the single-point calculations are also calculated at the B3LYP/TZVP theoretical level. All the stationary points along with the reaction coordinate have been performed via constraining optimizations and frequency analyses (no imaginary frequencies) to obtain the thermodynamic corrections in the corresponding electronic states. Zero-point energy corrections and thermal corrections to the Gibbs free energy have been also performed according to the harmonic vibrational frequencies.

Fine quadrature grids of size 4 were employed. The self-consistent field (SCF) convergence thresholds of the energy for both the ground state and excited state optimization were set at 10^{-8} (default settings are 10^{-6}). Harmonic vibrational frequencies in the ground and excited state were determined by diagonalization of the Hessian. The excited-stated Hessian was obtained by numerical differentiation of the analytical gradients using central differences and default displacements of 0.02 Bohr. The infrared intensities were determined from the gradients of the dipole moment.

3. Results and discussion

To confirm the stable configurations of ABO and ABT systems, the optimized geometrical structures of ABO-enol, ABO-keto (the proton-transfer ABO), ABT-enol and ABT-keto (the proton-transfer ABT) based on B3LYP/TZVP theoretical level have been shown in **Figure 1**. To the best of knowledge, the quantum theory of atoms in molecules (AIM) should be an effective manner to explore the formation of chemical bond [61-64], therefore, we firstly perform the AIM analyses about ABO and ABT system in the S_0 state. Given the AIM theory, identification of a critical point (CP) and the existence of a bond path in equilibrium geometry are necessary and sufficient conditions for assigning an interaction between two primary atoms. And the AIM analysis of the title compounds ensure the presence of an appreciable interaction in between the atoms concerned. The relevant AIM topological parameters involved in the optimized geometries show that the ρ(r) at the bond critical point (BCP) for the S_0-state ABO-enol and ABT-enol geometries are close to the 0.040 a.u. (the maximum threshold value proposed by Popelier to ensure the presence of hydrogen bond [62]). It justifies the presence of intramolecular hydrogen bond (N-H•••N) for both ABO-enol and ABT-enol, which is

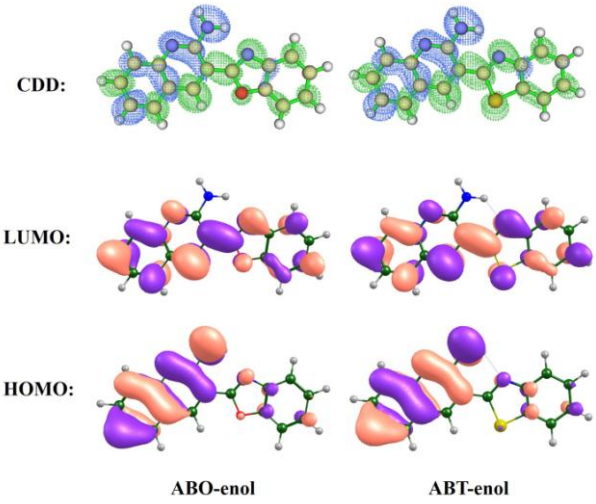

Figure 4: View of the relative frontier molecular orbitals (HOMO and LUMO) for ABO-enol and ABT-enol systems. The theoretical charge-density difference (CDD) maps between S_0 and S_1 states are also shown for both ABO-enol and ABT-enol structures. The regions with increasing electron density are shown in green, while the regions with decreasing density are shown in blue.

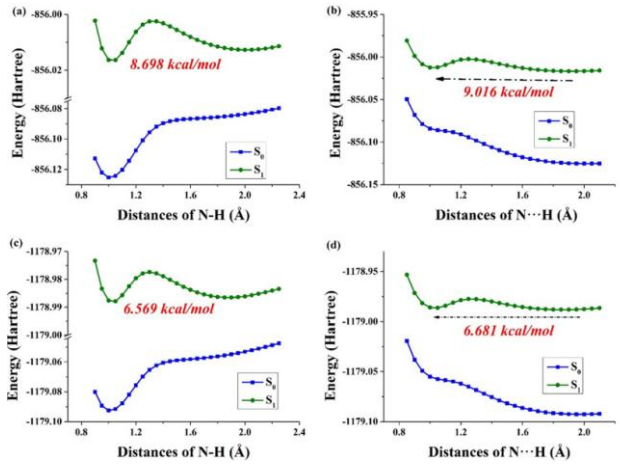

Figure 5: The constructed potential energy curves for both ABO (a) (b) and ABT (c) (d) in both S_0 and S_1 states. (a) Elongating the N-H single bond of ABO-enol structure in step of 0.05 Å; (b) Shortening the N•••H hydrogen bond of ABO-enol form in step of 0.05 Å; (c) Elongating the N-H single bond of ABT-enol form in step of 0.05 Å; (d) Shortening the N•••H hydrogen bond of ABT-enol form in step of 0.05 Å. The relative potential energy barriers in the S_1 states are shown.

further substantiated from the corresponding 2ρc value being well within the range (0.02 ~ 0.15 a.u.) [61-64]. Therefore, it can be further confirmed that hydrogen bond should be formed in the S0 state.

The primary structural parameters (bond lengths and bond angles involved in hydrogen bond moieties) of ABO-enol, ABO-keto, ABT-enol and ABT-keto have been listed in **Table 1**. Obviously, the optimized S_0-state ABO-keto and ABT-keto forms transform to the ABO-enol and ABT-enol structures, and it can be found clearly that the bond lengths and bond angles for ABO-keto and ABT-keto are the same as the ABO-enol and ABT-enol ones. From this aspect, we can infer that the S_0-state intramolecular proton transfer along with N-H•••N from ABO-enol to ABO-keto and from ABT-enol to ABT-keto should be unsupported. Furthermore, our theoretical results show that the bond length of N-H of ABO and ABT changes from S_0-state 1.010 Å (ABO-enol) and 1.011 Å (ABT-enol) to S_1-state 1.025 Å and 1.028 Å, respectively. And one should be noticed that the bond angle δ(N-H•••N) is also increased from S_0 state to the S_1 state. That is to say, the hydrogen bond N-H•••N should be strengthened in the S_1 state for both ABO and ABT systems based on the photo-excitation [65-77]. Moreover, spectral shift with special vibrational modes can be also used to detect the electronic excited-state hydrogen bond dynamics [65-77]. The S_0-state and S_1-state infrared (IR) vibrational spectra of ABO and ABT at the spectral region of N-H stretching band have been shown in **Figure 2**. It should be noted that the S0-state vibrational mode of N-H moiety for ABO-enol is located at 3516 cm^{-1}, whereas the first excited-state mode is located at 3307 cm^{-1}. Also for ABT-enol structure, a red shift 265 cm^{-1} can be lead to from S_0-state 3502 cm^{-1} to S_1-state 3237 cm^{-1}. This phenomenon indicates that the intramolecular hydrogen bond N-H•••N should be reinforced in the S_1 state [65-77]. Furthermore, according to the relationship between bond energy EHB and potential energy density V(r) at corresponding BCP could be approximately described as EHB=V(r)/2 [63], we also estimate the hydrogen bonding energies for ABO and ABT systems in both S_0 and S_1 states. The theoretical EHB of ABO-enol is calculated to be 6.33 kcal/mol in the S_0 state, and the EHB of S_1-state ABO-enol is around 9.34 kcal/mol. Also for ABT-enol structure, the S_0-state hydrogen bond energy is about 7.44 kcal/mol, while that of S_1 state is calculated to be 10.15 kcal/mol. Therefore, we confirm that the intramolecular hydrogen bond N-H•••N should be strengthened in the first excited state for both ABO and ABT systems, which may facilitate the ESIPT reactions.

To explore the photo-excitation process, our theoretical calculations predict the low-lying six absorbing transitions for both ABO and ABT systems. The absorption spectra have been obtained from the vertical excitation calculations based on the optimized S_0-state ABO-enol and ABT-enol forms. The emission spectra can be obtained from the optimized S_1-state structures. The relative absorption and fluorescence spectra have been shown in **Figure 3** to make a reasonable comparison with previous experimental results. It is worth mentioning that the theoretical absorption peak of ABO-enol is 389 nm, which is in agreement with experimental data (386 nm) [50]. The emission peak of ABO-enol configuration is around 444 nm, which is also consistent with experimental 455 nm [50]. And we predict the fluorescence peak of ABO-keto should be 714 nm, which is not reported in experiment since the range of steady-state in previous experiment are not beyond 650 nm. In the similar way, the absorption peak of ABT-enol is calculated to be 403 nm, which is close to 394 nm in experiment [50]. Also the emission peak of ABT-enol is around 463 nm consistent with experimental 469 nm. And the fluorescence of the proton-transfer ABT-keto is predicted to be 727 nm. All these agreements with previous experimental reports demonstrate that the theoretical excited state of ABO and ABT systems based on the TDDFT/B3LYP/TZVP theoretical level can delineate the excited-state characteristics well. It is well known that the changes about charge distribution bringing from the photo-excitation process are closely related to excited state dynamical behaviors [65-77], therefore, it is necessary to qualitatively explore the charge redistribution in electronic excited states. In this work, the charge distributions and charge transfers in the excited states are examined using the frontier molecular orbitals (MOs) methods. Based on our theoretical excitation process, we just show the highest occupied molecular orbital (HOMO) and the lowest unoccupied molecular orbital (LUMO) in **Figure 4**, since the S_0-S_1 transition for both ABO-enol and ABT-enol is mainly associated with these two orbitals. It can be found that the S1 state owns a distinct ππ* feature because of the π character for HOMO and π* character for LUMO. Clearly, they are localized in different moieties of ABO-enol and ABT-enol, which reveals the S_1 state should refer to charge transfer phenomenon. It cannot be denied that the charge density of N atom of the benzazole moieties increases for both ABO-enol and ABT-enol systems upon the transition from HOMO to LUMO, while that of N atom of the amino groups decreases.

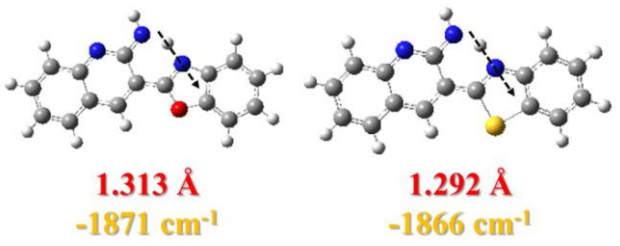

Figure 6: The S_1-state TS structures separating ABO-enol and ABO-keto as well as ABT-enol and ABT-keto structures. Herein, the vibrational eigenvector of TS form points to the correct ESIPT direction. The corresponding N-H bond distance and imaginary frequency for ABO and ABT have been also listed.

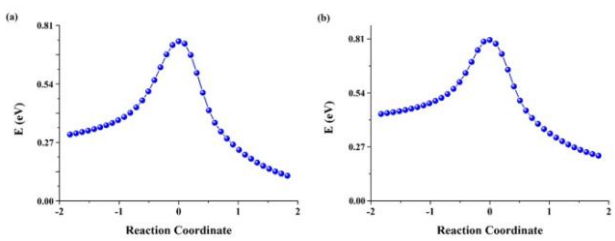

Figure 7: The energy profile along the excited state IRC for the ESIPT path for ABO (a) and ABT (b) systems based on TDDFT/B3LYP/TZVP theoretical level.

For more visual, the charge-density difference (CDD) maps are also shown in **Figure 4**. It indicates that upon the photoexcitation from S_0 to S_1 net charge densities shift from the hydroxyl moiety to N atom for ABO-enol and ABT-enol structures. In general, this kind of changes about charge density involved in intramolecular hydrogen bond can facilitate the ESIPT reaction [65-77].

In order to further clarify the detailed mechanism about the ESIPT reaction for both ABO and ABT systems, herein, the potential energy curves for ABO and ABT have been constructed in both S_0 and S_1 states. And the process of this kind of calculations is time-consuming, particularly for the S_1-state calculation. Nevertheless, the theoretical constructed can qualitatively explain the reaction mechanism along with the reaction path [65-77]. The constructed potential energy curves have been displayed in **Figure 5**. Herein, we adopt two kinds of manners to construct potential energy curves. In **Figure 5 (a)** and **Figure 5 (c)**, we elongate the N-H single chemical bond of ABO and ABT molecules in step of 0.05 Å, respectively. For **Figure 5 (b)** and **Figure 5 (d)**, we explore the ESIPT process via shortening the intramolecular hydrogen bond N•••H in step of 0.05 Å, respectively. And both initial normal ABO-enol as well as ABT-enol and the proton-transfer tautomers ABO-keto and ABT-keto structures are included in the curves. Clearly, the S_0-state potential energy curves for both ABO and ABT molecules are increased ceaselessly with the elongation of N-H single bond or shortening of hydrogen bond N•••H, which reveals the ground-state intramolecular proton transfer reactions cannot occur. While for the S_1 states, it can be found clearly that the ABO-enol and ABT-enol forms can be easily isomerized into the ABO-keto and ABT-keto tautomers by crossing low barriers. Subsequently, the S_1-state tautomer forms can go back to the S_0 state though emission, and then undergoes the reversed ground state intramolecular proton transfer from ABO-keto to ABO-enol and from ABT-keto to ABT-enol with the recovery of four-level reaction cycle.

To further verify the ESIPT mechanism for both ABO and ABT systems, using the Berny optimization method [78], we also search the transition state (TS) structures for both ABO and ABT systems. The corresponding results have been shown in **Figure 6**. All the TS structures have been confirmed to be only one imaginary frequency, and its vibrational eigenvector points to the ESIPT reaction directions. Then, the excited state reaction path is also constructed based on integrating the intrinsic reaction coordinate (IRC) at the same level of theory. The IRC results have been shown in **Figure 7**. This scheme of integration over the S_1-state PESs can be obtained by combining the first-order Euler predictor approach with a modified Bulrisch-Stoer integrator for the corrector algorithm [79-82]. Beginning from the TS structures, two minima (i.e., the reactants and products) have been searched according to the direction of energy decrease, respectively. Therefore, we can confirm the ESIPT mechanism we put forward in this work is reasonable.

4. Conclusions

In summary, in this present work, the properties about intramolecular hydrogen bond of two N-H type ESIPT molecules ABO and ABT have been investigated theoretically. Via AIM analyses, we firstly verify the formation of intramolecular hydrogen bond for both ABO and ABT molecules, which is the precondition of ESIPT reaction. Analyses the changes of hydrogen bonds between S_0 and S_1 states, we find hydrogen bond N-H•••N should be strengthened in the excited state via exploring bond lengths, bond angles and IR vibrational spectra. The strengthening N-H•••N provides the possibility for ESIPT process for ABO and ABT. Insight into charge redistribution of ABO and ABT upon photo-excitation, we demonstrate that the charge transfer phenomenon should be tendency of ESIPT. Via constructing potential energy curves of both S_0 and S_1 states using two kinds of methods, we clarify the ESIPT mechanism for ABO and ABT with elaborating the recovery of four-level reaction cycle. And the searching TS structures for ABO and ABT systems in the S_1 state along with the ESIPT path as well as the simulated IRC further confirm the ESIPT reaction.

Acknowledgements

This work was supported by the Natural Science Foundation of China (11604333), the Key Scientific Research Project of Colleges and Universities of Henan Province of China (18A140023 and 16B140002) and Science and Technology Research Project of Henan Province (172102210391).

References

[1] I. Alkorta, I. Rozas, J. Elguero, Chem. Soc. Rev. **1998**, 27, 163.
[2] L. Sobczyk, S. Grabowski, T. Krygowski, Chem. Rev. **2005**, 105, 3513.
[3] G. Gilli, P. Gilli, J. Mol. Struct. **2000**, 552, 1.
[4] G. Desiraju, Angew. Chem. Int. Ed. **2007**, 46, 8342.
[5] S. Grabowski, Chem. Rev. **2011**, 111, 2597.
[6] P. Song, F. Ma, Int. Rev. Phys. Chem. **2013**, 32, 589.
[7] B. Siwick, H. Bakker, J. Am. Chem. Soc. **2007**, 129, 13412.
[8] A. Weller, Prog. React. Kinet. **1961**, 1, 187.
[9] M. eigen, W. Kruse, G. Maass, L. Meayer, Prog. React. Kinet. **1964**, 2, 285.
[10] H. Tseng, J. Shen, T. Kuo, T. Tu, Y. Chen, A. Demchenko, P. Chou, Chem. Sci. **2016**, 7, 655.
[11] A. Demchenko, K. Tang, P. Chou, Chem. Soc. Rev. **2013**, 42, 1379.
[12] J. Zhao, P. Song, F. Ma, Commun. Comput. Chem. **2014**, 2, 117.
[13] Y. Liu, T. Chu, Chem. Phys. Lett. **2011**, 505, 117.
[14] Y. Liu, S. Lan, C. Zhu, S. Lin, J. Phys. Chem. A **2015**, 119, 6269.
[15] F. Yu, P. Li, G. Li, G. Zhao, T. Chu, K. Han, J. Am. Chem. Soc. **2011**, 133, 11030.
[16] J. Zhao, Y. Yang, Commun. Comput. Chem. **2016**, 4, 1.
[17] J. Zhao, J. Chen, J. Liu, M. Hoffmann, Phys. Chem. Chem. Phys. **2015**, 17, 11990.
[18] H. Yin, H. Li, G. Xia, C. Ruan, Y. Shi, H. Wang, M. Jin, D. Ding, Sci. Rep. **2016**, 6, 19774.
[19] K. Tang, C. Chen, H. Chuang, J. Chen, Y. Chen, Y. Lin, J. Shen, W. Hu, P. Chou, J. Phys. Chem. Lett. **2011**, 2, 3063.
[20] M. Zhang, Q. Zhou, C. Du, Y. Ding, P. Song, RSC. Adv. **2016**, 6, 59389.
[21] J. Zhao, H. Yao, J. Liu, M. Hoffmann, J. Phys. Chem. A **2015**, 119, 681.
[22] Y. Liu, M. Mehata, S. Lan, Spectrochimica. Acta. Part A **2014**, 128, 280.

[23] P. Chou, Y. Chen, C. Wei, W. Chen, J. Am. Chem. Soc. **2000**, 122, 9322.
[24] J. Huang, J. Zhang, D. Chen, H. Ma, Org. Chem. Front. **2017**, 4, 1812.
[25] H. Ma, J. Huang, RSC Adv. **2016**, 6, 96147.
[26] C. Hsieh, P. Chou, C. Shih, W. Chuang, M. Chung, J. Lee, T. Joo, J. Am. Chem. Soc. **2011**, 133, 2932.
[27] K. Tang, M. Chang, T. Lin, H. Pan, T. Fang, K. Chen, W. Hung, Y. Hsu, P. Chou, J. Am. Chem. Soc. **2011**, 133, 17738.
[28] J. Zhao, P. Song, F. Ma, Commun. Comput. Chem. **2015**, 2, 146.
[29] J. Huang, K. Yu, H. Ma, S. Chai, B. Dong, Dyes and Pigments, **2017**, 141, 441.
[30] G. Li, T. Chu, Phys. Chem. Chem. Phys. **2011**, 13, 20766.
[31] G. Li, G. Zhao, Y. Liu, K. Han, G. He, J. Comput. Chem. **2010**, 31, 1759.
[32] P. Chou, M. Martinez, W. Cooper, C. Chang, Appl. Spectrosc. **1994**, 48, 604.
[33] P. Chou, S. Studer, M. Martinez, Appl. Spectrosc. **1991**, 45, 513.
[34] X. Peng, Y, Wu, J. Fan, M. Tian, K. Han, J. Org. Chem. **2005**, 70, 10524.
[35] Q. Chu, Y. Pang, Macromolecules, **2002**, 35, 7569.
[36] P. Song, J. Ding, T. Chu, Spectrochimica. Acta Part A **2012**, 97, 746.
[37] J. Wang, Q. Chu, X. Liu, C. Wesdemiotis, Y. Pang, J. Chem. Phys. B **2013**, 117, 4127.
[38] S. Lim, J. Seo, S. Park, J. Am. Chem. Soc. **2006**, 128, 14542.
[39] T. Carter, M. Van Benthem, G. Gillispie, J. Phys. Chem. **1983**, 87, 1891.
[40] N. Allen, B. Harwood, J. Mckellar, J. Photochem. **1979**, 10, 187.
[41] T. Smith, K. Zaklika, K. Thakur, P. Barbara, J. Am. Chem. Soc. **1991**, 113, 4035.
[42] C. Fahrni, M. Henary, D. Van Derveer, J. Phys. Chem. A **2002**, 106, 7655.
[43] S. Santra, G. Krishnamoorthy, S. Dogra, J. Phys. Chem. A **2000**, 104, 476.
[44] M. Nayak, J. Photochem. Photobiol. A **2012**, 241, 26.
[45] A. Ciuciu, K. Skonieczny, D. Koszelewski, D. Gryko, L. Flamigni, J. Phys. Chem. C **2013**, 117, 791.
[46] J. Joule, K. Mills, Heterocyclic Chemistry, 5th ed.; Wiley-Blackwell: West Sessex, U.K. **2010**.
[47] H. Tseng, J. Liu, Y. Chen, C. Chao, K. Liu, C. Chen, T. Lin, C. Hung, Y. Chou, T. Lin, T. Wang, P. Chou, J. Phys. Chem. Lett. **2015**, 6, 1477.
[48] A. Stasyuk, Y. Chen, C. Chen, P. Wu, P. Chou, Phys. Chem. Chem. Phys. **2016**, 18, 24428.
[49] Y. Chen, F. Meng, Y. Hsu, C. Hung, C. Chen, K. Chung, W. Tang, W. Hung, P. Chou, Chem. Eur. J. **2016**, 22, 14688.
[50] M. Khimich, B. Uzhinov, Int. J. Photoenergy, **2006**, 206, 153.
[51] M. Khimich, V. Ivanov, M. Melnikov, B. Uzhinov, High Energy Chem. **2017**, 51, 17.
[52] M. Khimich, V. Ivanov, M. Melnikov, I. Shelaev, F. Gostev, V. Nadtochenko, B. Uzhinov, Phtotchem. Photobiol. Sci. **2017**, 16, 1139.
[53] C. Lee, W. Yang, R. Parr, Phys. Rev. B **1988**, 37, 785.
[54] W. Kolth, A. Becke, R. Parr, J. Phys. Chem. **1996**, 100, 129743
[55] F. Furche, R. Ahlruchs, J. Chem. Phys. **2002**, 117, 7433.
[56] M. J. Frisch, G. W. Trucks, H. B. Schlegel, G. E. Scuseria, M. A. Robb, J. R. Cheeseman, G. Scalmani, V. Barone, B. Mennucci, G. A. Petersson, H. Nakatsuji, M. Caricato, X. Li, H. P. Hratchian, A. F. Izmaylov, J. Bloino, G. Zheng, J. L. Sonnenberg, M. Hada, M. Ehara, K. Toyota, R. Fukuda, J. Hasegawa, M. Ishida, T. Nakajima, Y. Honda, O. Kitao, H. Nakai, T. Vreven, J. A. Montgomery Jr, J. E. Peralta, F. Ogliaro, M. Bearpark, J. J. Heyd, E. Brothers, K. N. Kudin, V. N. Staroverov, T. Keith, R. Kobayashi, J. Normand, K. Raghavachari, A. Rendell, J. C. Burant, S. S. Iyengar, J. Tomasi, M. Cossi, N. Rega, J. M. Millam, M. Klene, J. E. Knox, J. B. Cross, V. Bakken, C. Adamo, J. Jaramillo, R. Gomperts, R. E. Stratmann, O. Yazyev, A. J. Austin, R. Cammi, C. Pomelli, J. W. Ochterski, R. L. Martin, K. Morokuma, V. G. Zakrzewski, G. A. Voth, P. Salvador, J. J. Dannenberg, S. Dapprich, A. D. Daniels, O. Farkas, J. B. Foresman, J. V. Ortiz, J. Cioslowski and D. J. Fox, Gaussian 09, revision C.01; Gaussian, Inc., Wallingford, CT, **2009**.
[57] D. Feller, J. Comput. Chem. **1996**, 17, 1571.
[58] E. Cances, B. Mennucci, J. Tomasi, J. Chem. Phys. **1997**, 107, 3032.
[59] B. Mennucci, J. Tomasi, J. Chem. Phys. **1997**, 106, 5151.
[60] M. Cossi, V. Barone, B. Mennucci, J. Tomasi, Chem. Phys. Lett. **1998**, 286, 253.
[61] B. W. Bader, Atoms in molecules, a quantum theory, Clarendon Press, Oxford, U.K. **2000**.
[62] P. Popelier, J. Phys. Chem. A **1998**, 102, 1873
[63] E. Espinosa, E. Molins, C. Lecomte, Chem. Phys. Lett. **1998**, 285, 170.
[64] S. Noorizadeh, E. Shakerzadeh, Phys. Chem. Chem. Phys. **2010**, 12, 4742.
[65] G. Zhao, K. Han, Acc. Chem. Res. **2012**, 45, 404.
[66] H. Li, H. Yin, X. Liu, Y. Shi, M. Jin, D. Ding, Spectrochimica Acta Part A **2017**, 184, 270.
[67] J. Zhao, J. Chen, P. Song, J. Liu, F. Ma, J. Clust. Sci. **2015**, 26, 1463.
[68] G. Fan, K. Han, G. He, Chin. J. Chem. Phys. **2013**, 26, 635.
[69] Y. Dai, J. Zhao, Y. Cui, Q. Wang, P. Song, F. Ma, Y. Zhao, Spectrochimica Acta Part A **2015**, 144, 76.
[70] H. Li, H. Yin, X. Liu, Y. Shi, J. At. Mol. Sci. **2016**, 7, 115.
[71] K. Han, G. He, J. Photochem. Photobiol. C **2007**, 8, 55.
[72] Y. Cui, Y. Li, Y. Dai, F. Verpoort, P. Song, L. Xia, Spectrochimica Acta Part A **2016**, 154, 130.
[73] C. Miao, Y. Shi, J. Comput. Chem. **2011**, 32, 3058.
[74] Q. Wei, Q. Zhou, M. Zhao, M. Zhang, P. Song. J. Lumin. **2017**, 183, 7.
[75] Y. Cui, H. Zhao, L. Jiang, P. Li, Y. Ding, P. Song, L. Xia, Comput. Theor. Chem. **2015**, 1074, 125.
[76] J. Zhao, P. Song, Y. Cui, X. Liu, S. Sun, S. Hou, F. Ma, Spectrochimica Acta Part A **2014**, 131, 282.
[77] Y. Wang, Y. Shi, L. Cong, H. Li, Spectrochimica Acta Part A **2015**, 137, 913.
[78] H. B. Schlegel, J. Comput. Chem. **1982**, 3, 214.
[79] K. Fukui, Acc. Chem. Res. **1981**, 14, 363.
[80] C. Gonzalez, H. B. Schlegel, J. Chem. Phys. **1989**, 90, 2154.
[81] H. B. Schlegel, J. Chem. Soc. Faraday Trans. **1994**, 90, 1569.
[82] H. Hratchian, M. Frisch, H. Schlegel, J. Chem. Phys. **2010**, 133, 224101.